

Curvature attribute applications to 3D surface seismic data

SATINDER CHOPRA, Arcis Corporation, Calgary, Canada

KURT MARFURT, University of Houston, USA

Identifying subtle faults at or below the limits of seismic resolution and predicting fractures associated with folds and flexures is one of the major objectives of careful seismic interpretation. With the advent of common use of 3D seismic in the late 1980s, first-derivative-based horizon dip magnitude and dip azimuth were found to enhance faults that were otherwise difficult to see. More recently, second-derivative-based curvature maps have carried this process a step further. Horizon-based curvature computation is now available in the commercial workstation environment, putting these tools in the hands of geoscientists who do not have access to processing software and do not have time or inclination to program.

Background. Seismic interpreters have used attribute maps for fault interpretation since the introduction of 3D seismic data. As far back as 1991, Rijks and Jaufred showed that dip magnitude and dip azimuth can illuminate subtle faults having a displacement significantly less than the size of a seismic wavelet. Coherence (Bahorich and Farmer, 1995) and Sobel-filter-based edge detectors (Luo et al., 1996) measured lateral changes in seismic waveforms and amplitude. More recently, curvature attributes have been found to be useful in delineating faults and predicting fracture orientation and distribution (Roberts, 2001; Hakami et al., 2004). There are different curvature measures that can be used, each having its own characteristic property. Lisle (1994) discussed the correlation of Gaussian curvature to open fractures measured on an outcrop. Hart (2002) showed that strike curvature is highly correlated to open fractures in northwestern New Mexico. In contrast, Stevenson (personal communication, 2006) found that the dip component of curvature is correlated to open fractures in the Austin Chalk Formation of Central Texas.

Ericsson et al. (1988) demonstrated the relationship between production and curvature. While direct prediction of open fractures using curvature requires a significant amount of calibration through the use of production, tracer, image log, or microseismic measurements, curvature images also serve as a powerful aid to conventional structural and stratigraphic interpretation. Curvature is particularly useful in mapping faults that are smeared due to inaccurate migration. Sigismondi and Soldo (2003) have used larger

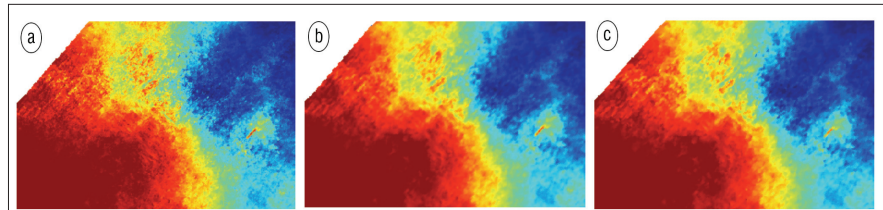


Figure 1. Impact of filters on a picked horizon. (a) Horizon picked on a 3D seismic volume from Alberta. (b) Horizon in Figure 1a with one pass of a mean filter. (c) Horizon in 1a with one pass of a median filter (data courtesy of Arcis Corporation).

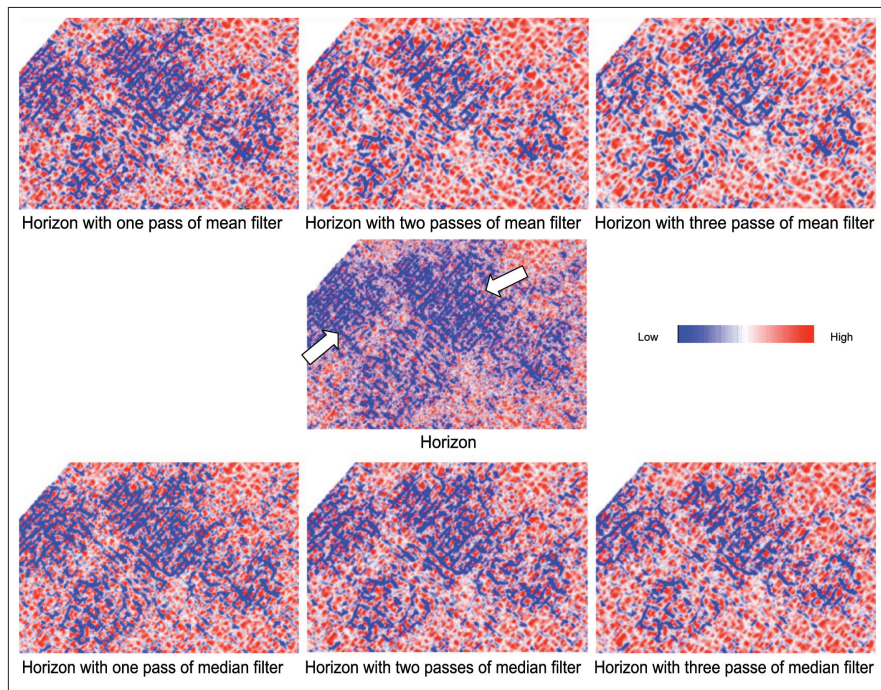


Figure 2. Impact of filters on the most-negative curvature computation. (center row) Most-negative curvature computed on the seismic horizon shown in Figure 1a. (top row) Most-negative curvature computed on the seismic horizon in Figure 1a with one, two, and three passes of mean filter. (bottom row) Most-negative curvature computed on the seismic horizon in Figure 1a with one, two, and three passes of median filter (data courtesy of Arcis Corporation).

analysis windows, thereby computing maximum curvature at different scales to extract subtle features that are much less obvious from the original time/structure map. Bergbauer et al. (2003) also compute curvature at different wavelengths by filtering the input horizon picks in k_x - k_y space. Al-Dossary and Marfurt (2006) extend this latter concept to volumetric estimates of curvature by replacing the k_x - k_y filter with a more tractable x - y convolutional operator.

While volumetric curvature has several significant advances over horizon-based curvature, not least of which is circumventing the need to pick regions through which no continuous surface exists, we understand that most interpreters do not have access to such processing software and

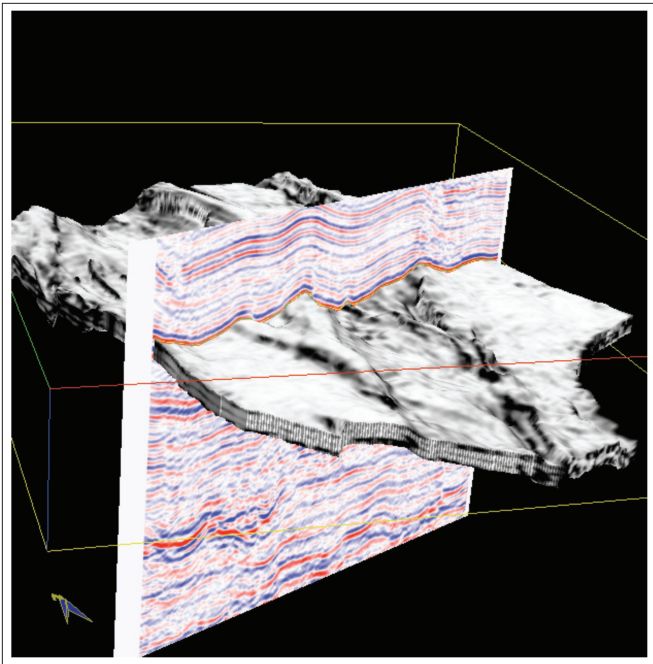


Figure 3. Coherence strat-cube shown intersected by a seismic inline (800 ms of data displayed) for a seismic volume from central-north British Columbia, Canada. The size of the survey displayed is 100 km² (data courtesy of Arcis Corporation).

computer power. In this paper, we therefore attempt to discuss how to use convenient filtering and display techniques available on modern interpretation software to generate horizon-based curvature estimates of similar quality to horizon slices through volumetric estimates.

We illustrate these workflows and discuss their usefulness in terms of their applications to two 3D seismic volumes, one from Alberta and the other from British Columbia, Canada.

Definition and types of curvature. Curvature can be defined as the reciprocal of the radius of a circle that is tangent to the given curve at a point. Thus curvature will be large for a curve that is “bent more” and will be zero for a straight line. Mathematically, curvature may simply be defined as a second-order derivative of the curve. If the radii of the circles at the point of contact on the curve are replaced by normal vectors, it is possible to assign a sign to curvature for different shapes, as was proposed by Roberts (2001). Diverging vectors on the curve are associated with anticlines, converging vectors with synclines, and parallel vectors with planar surfaces (which have zero curvature).

The concept of curvature can be conveniently extended to three-dimensional surfaces by considering such a surface being intersected by a plane and describing a curve. Curvature can then be calculated at any point on this curve. If a surface is cut by planes that are orthogonal to it, the curvature measures are referred to as normal curvatures (Roberts, 2001). Of the family of curves formed this way, there exist just two curves perpendicular to each other—one representing the maximum and the other the minimum curvature. Both, with their sign and magnitude, are useful, as faults can be clearly seen on such displays.

Curvature computation in practice. For most interpreters operating on a workstation, curvature is usually computed by fitting a quadratic surface $z(x, y)$ of the form

$$z(x, y) = ax^2 + cxy + by^2 + dx + ey + f \quad (1)$$

to an interpreted horizon using least-squares or some other approximation method. This yields the coefficients in Equation 1 from which other curvature measures can be derived, such as minimum and maximum curvatures, principal curvatures, most-positive, most-negative, dip curvature, strike curvature, curvedness, and shape index. Because curvature is a second derivative of the picked surface, its application to interpreted horizons needs to be done carefully in that it tends to exacerbate the finer detail and the noise as well. Horizons picked on noisy surface seismic data or data contaminated by mis-picks could lead to misleading curvature measures. Consequently, it is advisable to run spatial filtering on horizon surfaces, taking care to remove noise while retaining geologic detail. Most commercial software provides a basic suite of spatial filters that could be used for this purpose including mean, median, directional derivative, and sharpening.

The mean filter removes random noise and computes the mean or average of the values that fall within the chosen aperture. The mean filter applied to an interpreted surface enhances long-wavelength and suppresses short-wavelength curvature components. Iterative application of a mean filter to a map (i.e., applying the filter successively) will enhance longer and longer wavelength features. Conversely, if we subtract this long-wavelength map from the original broadband wavelength map and then compute curvature on the residual, we obtain curvature images that enhance short-wavelength features.

The median filter also removes random noise but preserves edges, which in the case of a picked horizon will include discrete offsets, such as encountered at a fault. The median filter can also be applied iteratively, which will reduce random noise in each iteration but will not significantly increase the high frequency geologic component of the surface.

Derivative (sometimes called Sobel) filters increase the high-frequency content of the data, and are commonly computed using a 3×3 mask oriented in a particular direction as shown below:

N-S direction:			E-W direction:		
+1	+2	+1	-1	0	+1
0	0	0	-2	0	+2
-1	-2	+1	-1	0	+1

Because curvature is a second-derivative operation applied to an interpreted surface, adding an additional derivative only further exacerbates any noise problems.

The sharpening (also call Laplacian) filter computes the second derivative of the inline and crossline components of dip and adds the results. Inspection of the formula provided by Roberts will show that the sharpening filter is closely related to the mean curvature, discussed below.

To illustrate these filters, we manually picked (line by line) a horizon surface that represents a limestone marker from a 3D volume from south central Alberta (Figure 1a). Care was taken to make certain there were no mis-picks. We then computed most-negative curvature of this surface without filtering (center panel of Figure 2). Note patches showing a discrete mesh of faults (white arrow). This horizon was successively passed through a 3×3 mean filter (Figure 1b) and the most-negative curvature generated in each pass. As seen in the upper panel of Figure 2, with each successive pass of the mean filter the background jitter is reduced and focusing of events increases. The same process was repeated with a 3×3 median filter (Figure 1c), and the corresponding images are shown in the lower panel of Figure 2. As

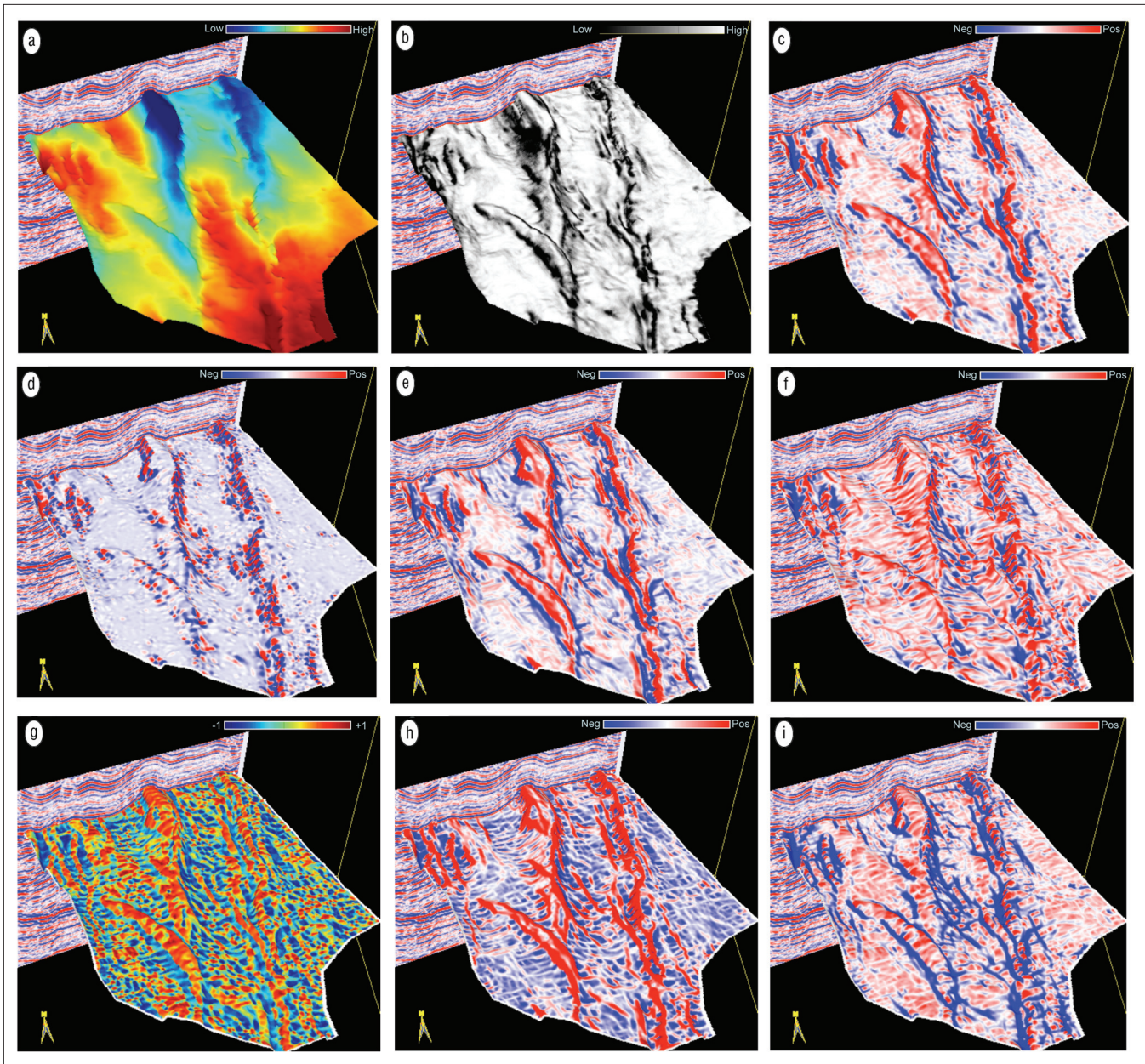


Figure 4. (a) Horizon time surface. (b) Coherence. (c) Mean curvature. (d) Gaussian curvature. (e) Dip curvature. (f) Strike curvature. (g) Shape index. (h) Most-positive curvature. (i) Most-negative curvature. The size of the survey displayed is 100 km². Approximately 800 ms of data are displayed on the vertical seismic section (data courtesy of Arcis Corporation).

expected, the median filter smooths random oscillations but preserves the major edges in the horizon time/structure map, resulting in crisper most-negative curvature displays.

Picking the horizon for accurate curvature computation.

Blumentritt (2006) found that the quality of volumetric estimates of curvature (that precomputed dip and azimuth volumes using a finite vertical analysis window of say, +/- 10 ms) could be approached better by picking the zero crossing. He explains this improvement in that noise added to the flat part of a peak or trough can significantly move the autopick. The same noise added to the much steeper zero crossing has a much smaller effect. We recommend the following workflow: (1) pick the data peak or trough as fits your well tie; (2) compute the quadrature of the seismic data; (3) snap the original picks to the zero crossing; (4) compute the curvature from these snapped picks to the zero crossings.

Because the data at the peak or trough are nearly flat,

moving them slightly will not significantly impact the amplitude extractions.

Curvature attributes. In this section, we will discuss the application of various curvature attributes to three examples.

Example 1. Figure 3 shows a coherence strat-cube being intersected by a seismic line from a 3D seismic volume from central-north British Columbia, Canada. A strat-cube is a sub-volume of seismic data or attributes that are either parallel to a picked horizon (commonly called a *flattened subvolume*) or interpolated at equal time increments between two non-parallel picked horizons.

A number of faults can be seen on the vertical seismic section. The top of the coherence strat-cube was chosen to be the base of Belloy Formation (Figure 4a). We illustrate the basic curvature attributes along the picked Belloy in Figures 4b–d:

Mean curvature is defined as the average of the minimum

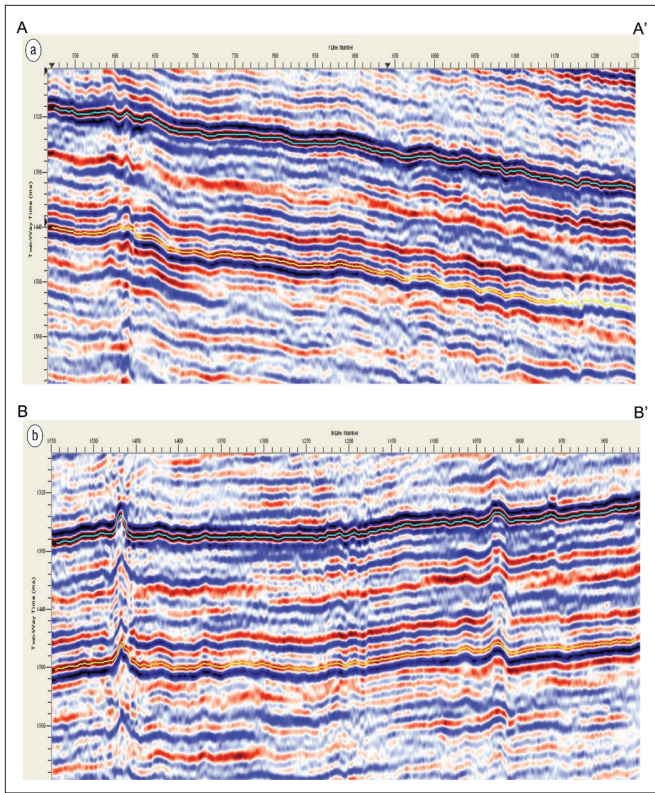


Figure 5. (a) Inline AA' and (b) crossline BB' from a 3D seismic volume from northwest Alberta. Two horizons were tracked on this volume, and the upper one was considered for curvature analysis (data courtesy of Arcis Corporation).

and maximum curvature and usually dominated by maximum curvature. Visually, it may not convey any additional information but is useful as other attributes are derived from it. Compared with coherence (Figure 4b), the sign of mean curvature indicates the high and low shapes (Figure 4c), giving a feel for the throw of the faults. Many like the fact that they can estimate fault throw by the change in color pattern (e.g., Sigismundi and Soldo).

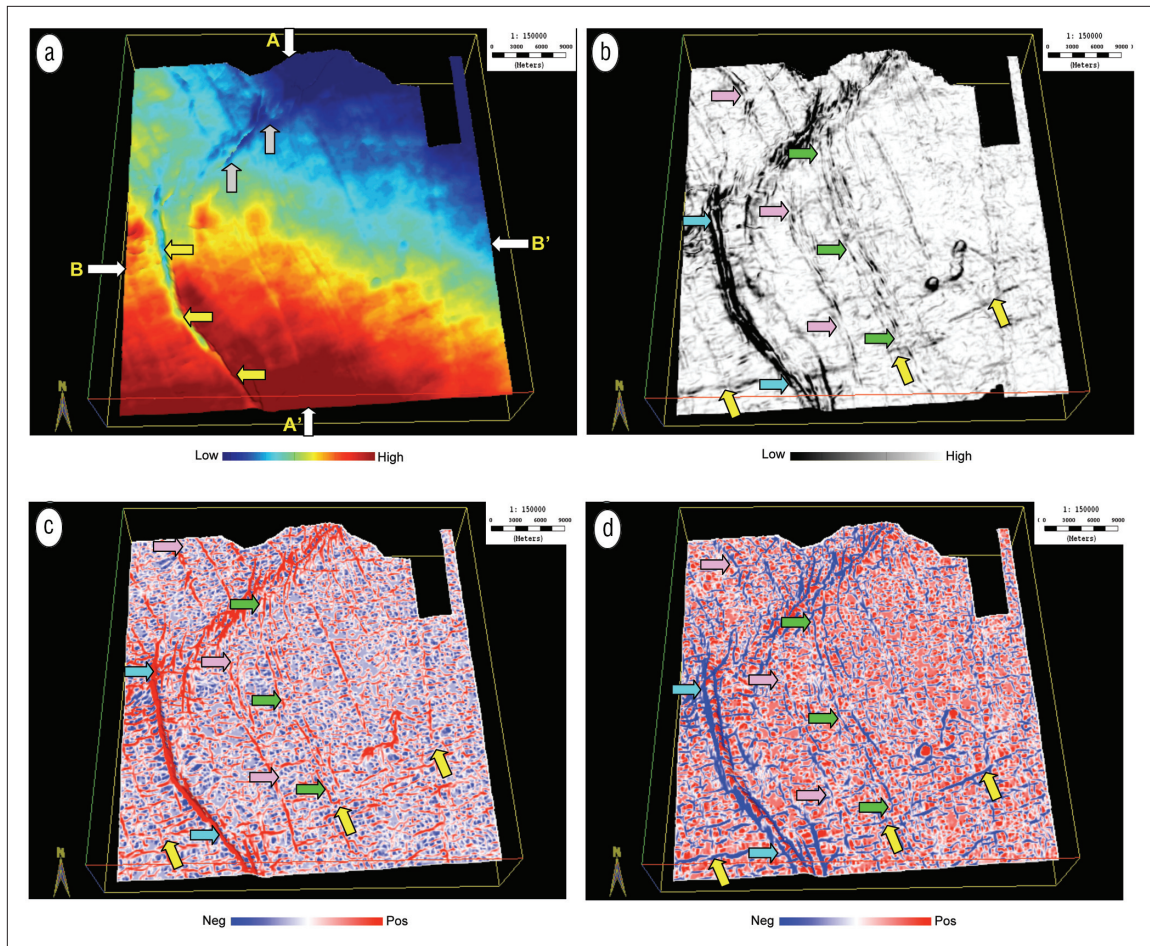
Gaussian curvature is defined as the product of the minimum and maximum curvatures and gives a measure of distortion of a surface. While this measure has been shown to be correlated to fractures (Lisle, 1994), it does not show discrete faults in this example (Figure 4d) or in the example presented by Roberts (2001).

Dip curvature is the curvature extracted along the direction of dip at each analysis point and measures the rate of change of dip in the maximum dip direction. As seen in Figure 4e, dip curvature clearly shows the throw and the direction of the faults. Stevenson finds that dip curvature is correlated to open fractures in extensional terrains.

Strike curvature is the curvature extracted along a direction perpendicular to the dip curvature (i.e., along strike at each analysis point). In Figure 4f, notice how the strike curvature indicates patterns connecting high with lows on both sides of the main fault. In a compressional terrain, Hart et al. (2002) predict that large values of strike curvature will be correlated to open (versus closed) fractures. In a tensional terrain such as the Austin Chalk, others find that dip curvature correlates with open fractures.

Shape index indicates the local shape of a surface with blue indicating a bowl, cyan a valley, green a saddle, yellow a ridge, and red a dome (Figure 4g). This attribute is

Figure 6. (a) Horizon time surface. (b) Equivalent coherence display. (c) Equivalent most-positive curvature display. (d) Equivalent most-negative curvature display. The size of the survey displayed is about 400 km². Block arrows (in different colors) indicate the lineaments as seen on different attribute displays (data courtesy of Arcis Corporation).



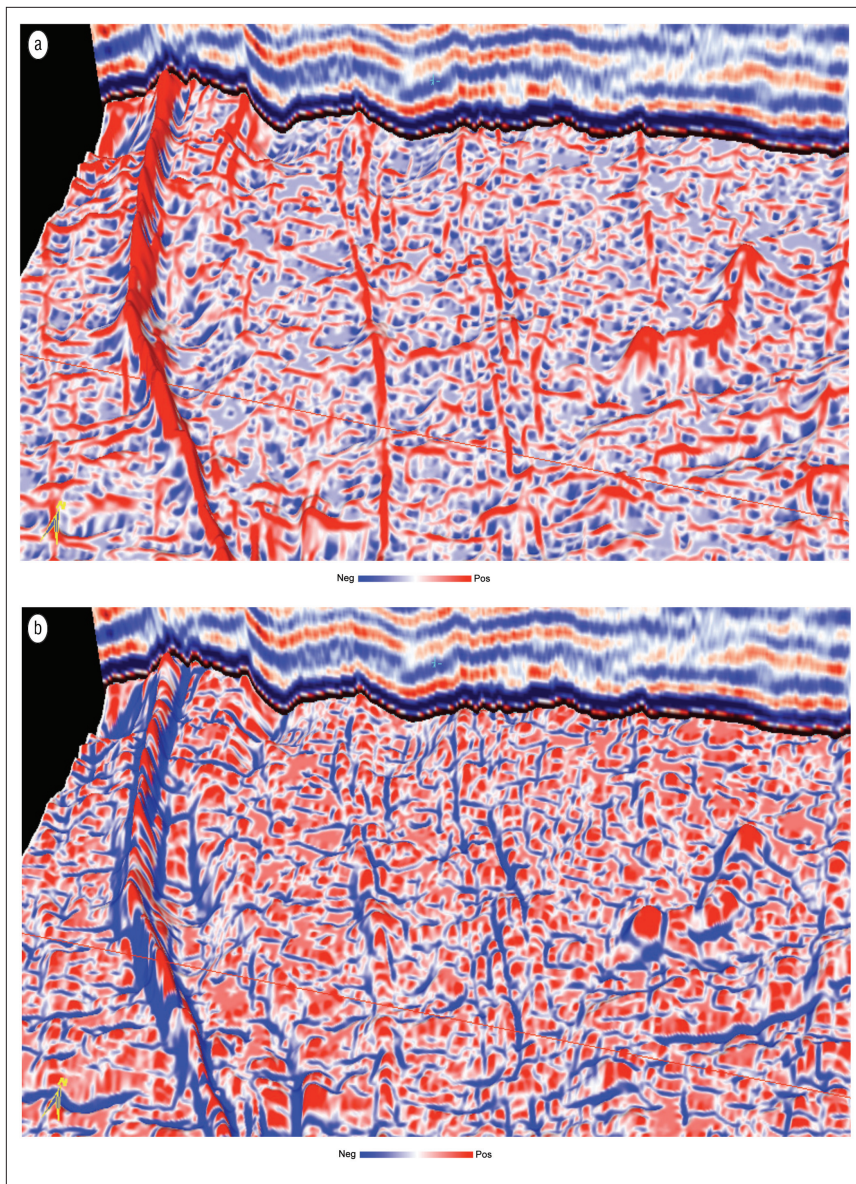


Figure 7. (a) Zoom of the most-positive curvature attribute horizon slice shown intersected with a seismic crossline. Notice that the peaks of the upthrown fault planes coated gray correlate with the bumps in the horizon times on the seismic horizon (data courtesy of Arcis Corporation). (b) Zoom of the most-negative curvature attribute horizon slice shown intersected with a seismic crossline. Notice that the peaks of the downthrown fault planes coated gray correlate with the lows in the horizon times on the seismic horizon (data courtesy of Arcis Corporation).

scale independent, meaning that gentle domes and strong domes will have a similar appearance.

Most-positive curvature defines the curvature that has the greatest positive value and will show anticlinal and domal features. However, negative values of the most positive curvature indicate a bowl feature (Figure 4h).

Most-negative curvature defines the curvature that has the greatest negative value and will in general highlight synclinal and bowl features. However, positive values of the most-negative curvature indicate a dome feature (Figure 4i).

Example 2. Figure 5a shows an inline and a crossline from a 3D seismic volume acquired in northwest Alberta for which we have picked two horizons and generated horizon-based curvature attributes. The upper time surface corresponding to the cyan horizon shown in Figure 5 is shown in Figure 6a and indicates two prominent fault trends, one at the top trending northeast–southwest (gray arrows) and

the other to the left trending northwest–southeast (yellow arrows). Figure 6a also indicates the positions of the two profiles in Figure 5. While there are hints of other faults, they do not appear as clearly. The corresponding horizon slice through the coherence volume (Figure 6b) shows the faults much better. However, the most-positive and most-negative displays computed from the picked horizon (Figure 6c and d) show the enhanced definition of the main fault trends with greater focus and clarity. Notice the finer definition of the faults indicated with yellow arrows and also the detail and density of the other features marked with cyan, pink, and green arrows. Figure 7a is a zoom of the most-positive curvature horizon slice seen intersected with a seismic crossline. Notice how the red peak on the fault trend (to the left running almost north–south) correlates with the upthrown signature on the seismic. Similarly, a zoom of the most-negative curvature horizon slice intersected with an inline (Figure 7b) shows the downthrown edges on both sides of the faults (highlighted in blue). Other similar features tend to stand out on the horizon slice.

Example 3. Besides faults/fractures, other stratigraphic features also appear well-defined on curvature displays. Figure 8a is a time surface from a 3D seismic survey in Alberta, depicting a meandering channel which is the most prominent feature that can be noticed on the display. The equivalent coherence display (Figure 8b) shows a crisper definition for the channel and other features, such as the lineament indicated with yellow arrows. The equivalent most-positive curvature display (Figure 8c) has a more focused and clear image of the linear feature. The cyan arrow indicates the well-defined lower leg of the channel on the curvature displays, which is not seen clearly on the coherence display. The edges of the meandering channel are well defined on the most-positive curvature display while the thalweg of the channel can be followed clearly on the most-negative display (Figure 8d).

It is important to couple the appearance of structural and stratigraphic features to a geologic model. In Alberta, some rocks are sufficiently old (Paleozoic to deeper Mesozoic) to have undergone differential compaction. Curvature is also successful in imaging subtle Mesozoic channels in the North Sea that have also undergone differential compaction (Helmire et al., 2004). In contrast, curvature rarely indicates channels in younger Tertiary sediments in surveys acquired in the Gulf of Mexico, where the rocks have not had time to undergo sufficient differential compaction.

Volume computation of curvature. Volume computation of curvature produces multispectral estimates of reflector curvature (Al Dossary and Marfurt, 2006). The method consists of choosing a moving subvolume of data to compute curvature at every point in the 3D seismic volume. As the first step, spurious events are minimized within the subvolume

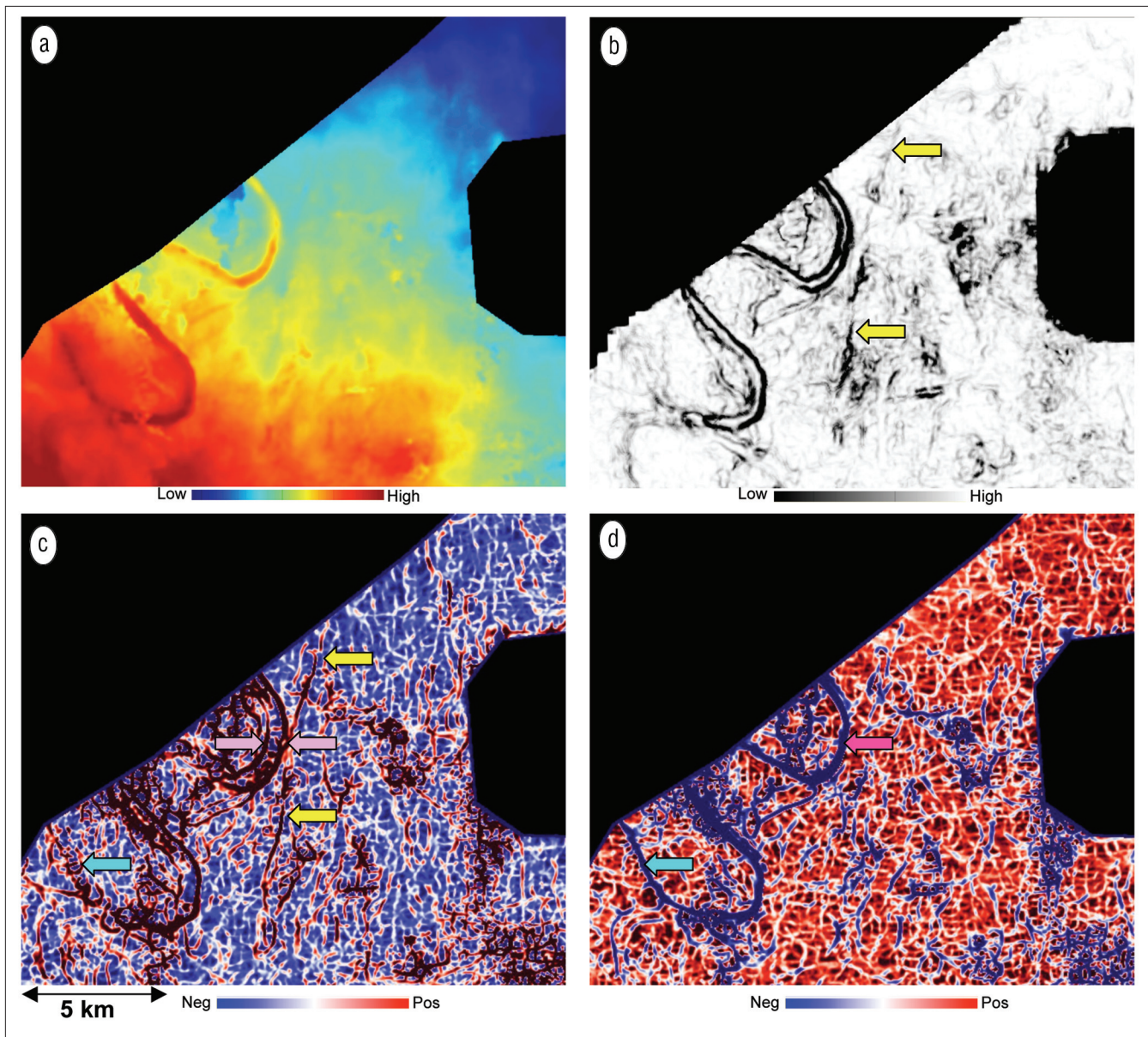


Figure 8. (a) Time surface. (b) Coherence. (c) Most-positive curvature. (d) Most-negative curvature. Curvature attributes indicate a better focusing of the base and edges of the channels and other features as compared with coherence. Yellow arrows indicate a linear feature on the coherence, but the same feature appears crisper on the most-positive curvature display. Cyan arrow indicates the well-defined lower leg of the channel on the curvature displays, which is not seen clearly on the coherence display. The edges of the meandering channel are defined well throughout the most-positive curvature display and the base of channel can be followed clearly on the most-negative display (data courtesy of Arcis Corporation).

and dip components are computed. Next, fractional derivatives are computed within the subvolume to investigate multiple wavelengths of curvature; short wavelengths correspond to intense, but highly localized fracture systems, and longer wavelengths to a wider and even distribution of fractures. Short-wavelength estimates of curvature could incorporate dip information of 9–25 traces; the long-wavelength estimates of curvature could use dip information of 400 or more traces. Fractional derivatives are thus applied along each time slice with dip components previously estimated at each seismic bin to yield estimates of curvature.

Volume curvature estimates eliminate interpretation problems and allow us to extract curvature measures along horizons, thereby helping understand the subsurface features better.

Example 1. Figure 9a shows the strat-slice from the most-positive curvature volume 30 ms below the horizon in Figure 4. The horizon at this level is not easy to track and so the

attribute volume helps in studying the fault patterns at this level. Similarly, the equivalent strat-slice extracted from the most-negative curvature volume is shown in Figure 9b. Notice, the fault pattern is somewhat different at this level, and these patterns can be studied carefully in the zone of interest.

Example 2. This example is from a survey over the Central Basin Platform of West Texas. The major production in this area is from the Devonian-age Thirty-one Formation, a chert deposit carried from the shelf in the north by turbidity flows into this deeper part of basin. The reservoir is highly compartmentalized and is enhanced by fractures. Figure 10a is an image of the most-positive curvature extracted along the yellow Thirty-one Formation horizon posted on the vertical slice through the seismic data. Figure 10b is an enlarged view of the seismic data corresponding to a producing part of the reservoir (green box in Figure 10a). Green arrows indicate synclinal and red arrows anticlinal features within this

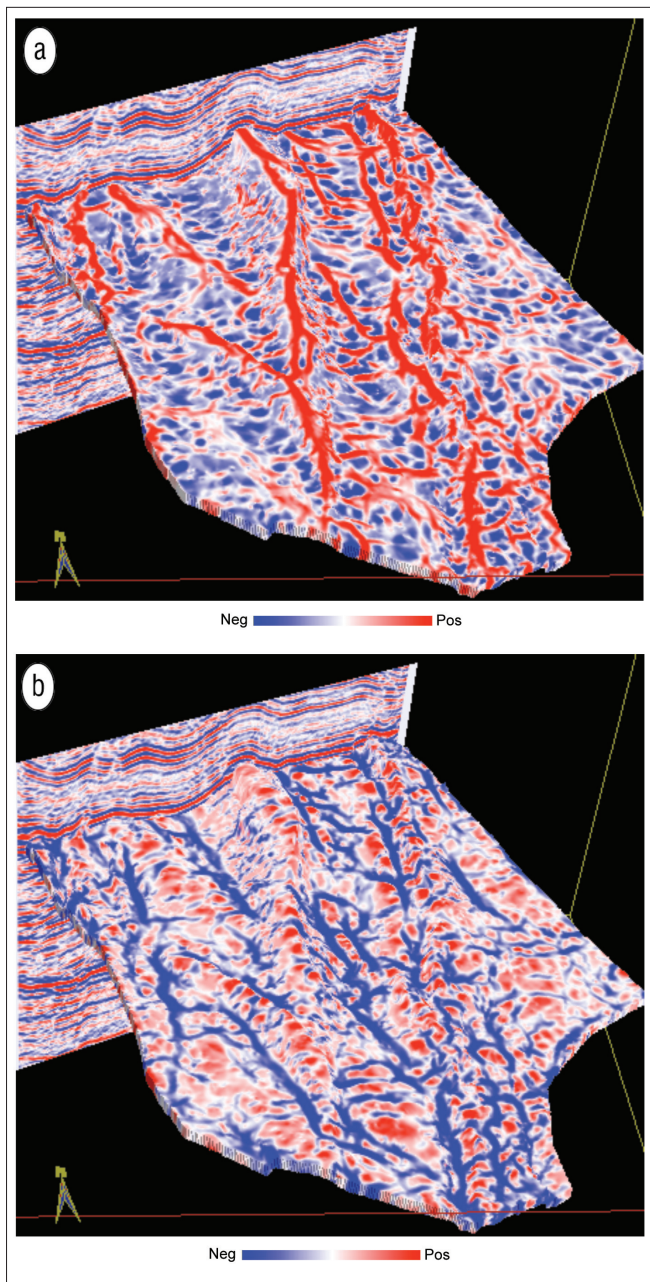


Figure 9. (a) Most-positive curvature strat-slice 30 ms below the tracked horizon surface extracted out of the curvature volume. (b) Most-negative curvature strat-slice 30 ms below the tracked horizon surface extracted out of the curvature volume (data courtesy of Arcis Corporation).

structural high. Figure 11 is the time/structure map of the yellow Thirty-one Formation pick in Figure 10a, and the corresponding coherence extraction (horizon slice through the coherence volume).

Figure 12 shows corresponding horizon slices through the most-negative and most-positive curvature volumes. Green and red arrows correspond to those in Figure 10b. Note that the subtle warping on the vertical seismic can be carried along the entire horizon, providing constraints on the paleo stress environment and possible fractures. The coherence extraction is relatively featureless over the zone of interest while the curvature volume is not. This reinforces our major point that coherence and curvature volumes are different because they are measuring different attributes of the input seismic volume. In particular, curvature shows

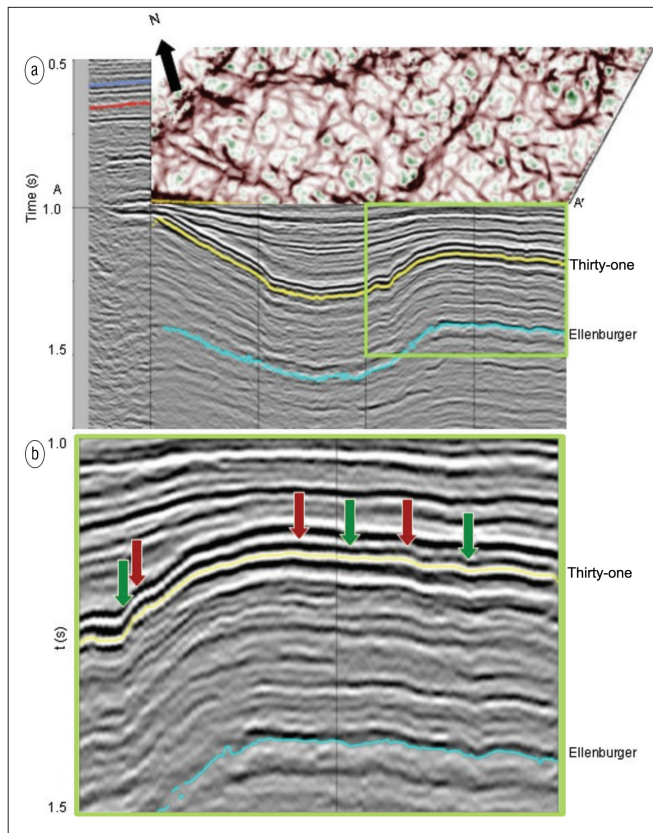


Figure 10. (a) A vertical slice through the seismic data of a horizon slice along the yellow Thirtyone Formation from the most-positive curvature volume. (b) Enlargement of the seismic data shown in the green box in Figure 10a. Note how the flexures seen on the seismic can be carried through the volume on the horizon slice through the most-positive curvature volume (after Marfurt, 2006).

subtle (unbroken!) flexures not seen by coherence because coherence is sensitive only to lateral discontinuities. In contrast, Figure 16 shows images in which coherence will delineate channels and (in the absence of differential compaction) curvature will not. The curvature computations are volumetric rather than along a surface. This is illustrated in Figure 13 which shows time slices at 1.0 s through the most-negative and positive curvature volumes. The posted yellow picks correspond to the intersection with the structurally deformed Thirty-one Formation.

Figures 14 and 15 more explicitly illustrate the correlation of these curvature computations to the original seismic data, coherence, most-negative curvature, and most-positive curvature. These curvature images provide the interpreter with a means of mapping local highs (domes) and lows (bowls) as well as carrying subtle flexures across the entire survey.

Curvature versus coherence. Seismic attributes—including rms amplitude, spectral decomposition, and geometric attributes—are all computed in a vertical analysis window and remove much of overprint of the seismic wavelet from the image. The polarity of a channel reflection depends not only on the impedance of the channel fill (which changes within the channel system) but also on the impedance of lithologies that underlay and overlay it. Attributes that remove the seismic wavelet generate images that are more visually consistent to the interpreter when seen on map view. Attribute vertical analysis windows on the order of the dominant period of the seismic data also improve the

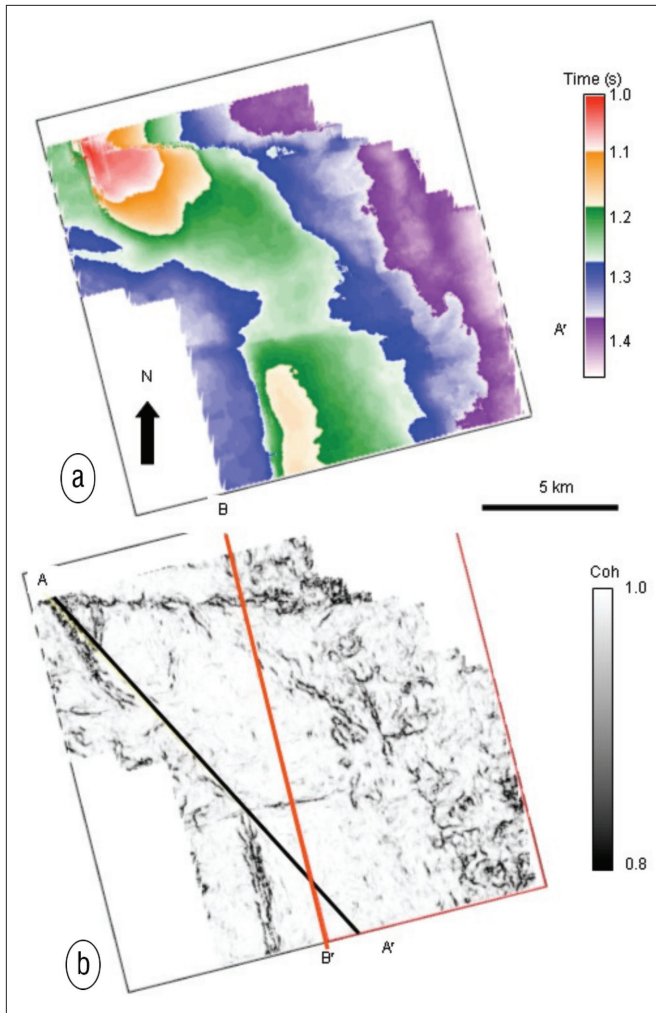


Figure 11. (a) Time/structure map and (b) a horizon slice through the coherence volume along the yellow Thirty-one Formation pick shown in Figure 10a (after Marfurt, 2006).

signal-to-noise (S/N) ratio of the image by stacking the information content of similar time slices together. However, vertical analysis windows much greater than the dominant period run the risk of mixing uncorrelated information from overlying and underlying strata.

Figure 16 presents three alternative models of how a channel may appear on different seismic attributes. Figure 16a shows a thin, flat-topped, channel below the tuning thickness. Observe that there will be no change in seismic waveform across this event, and it will not be seen by coherence. However, the channel will be seen by rms amplitude (and other energy measures), spectral decomposition, and coherent energy gradients. Figure 16b shows a thin channel that has undergone differential compaction. This channel will not result in a coherence anomaly but will be seen by attributes sensitive to amplitude, and because it deforms the (thicker) sediments above it, will now be seen as a most-positive curvature anomaly. Figure 16c shows a thicker channel, above thin-bed tuning. The right side of the channel will be seen by coherence because the waveform of the composite reflection will change abruptly. The left side of the channel will be seen where it cuts an underlying reflector. The gentle taper will in general not be seen by coherence because the change takes place over a lateral area larger than the analysis window. The reflection from the bottom of the channel may be broken due to lateral varying impedance

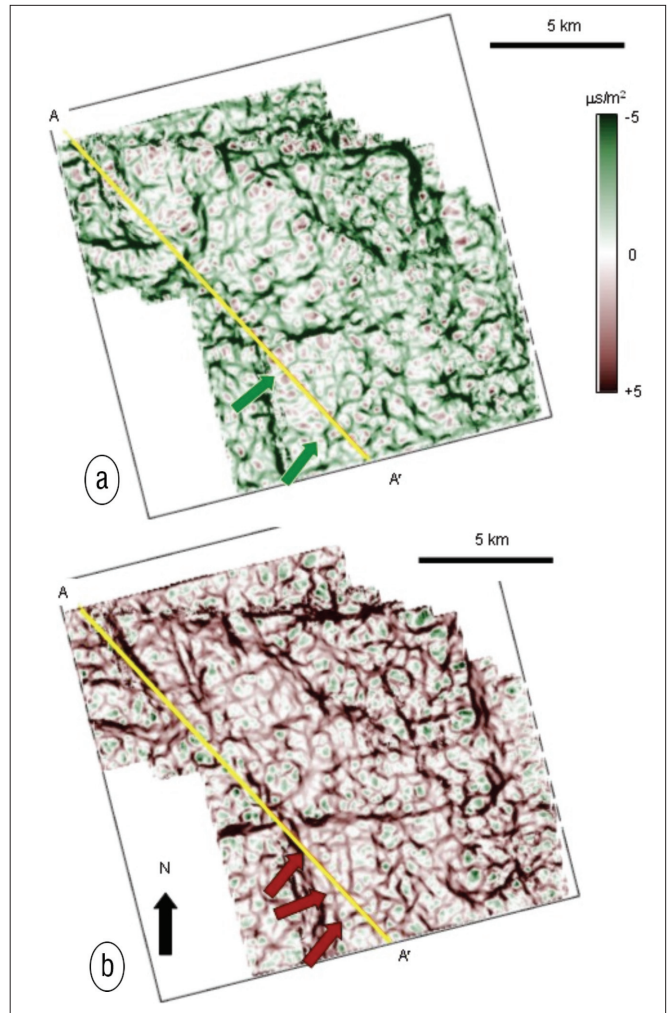


Figure 12. (a) Most-negative and (b) most-positive curvature extractions along the yellow Thirty-one Formation pick shown in Figure 10a and corresponding to the images shown in Figure 11. Note the added detail provided by the curvature volumes in areas where the coherence is featureless (after Marfurt, 2006).

and may not generate an accurate estimate of geologic dip. This channel will probably not be seen by curvature attributes. Finally, Figure 16d shows a thicker channel that is aggradational in form. It will be seen by our full suite of attributes.

Curvature attributes for well-log calibration. Figure 17 shows a phantom horizon slice extracted from the most-negative curvature volume at a level 120 ms below the horizon in Figures 4 and 9. The ability to display curvature along time slices, phantom horizon slices, and stratal slices that have not been explicitly picked is one of the major advantages of volume-based over horizon-based curvature computations. The individual lineaments in the three compartments formed by the two main faults running north-south have been tracked in three different colors. The orientations of these lineaments in the three compartments have been combined in the form of rose diagrams that retain the color of the lineaments. These rose diagrams can be compared with similar diagrams obtained from Formation Micro-Imager data to gain confidence in calibration. Once a favorable match is obtained, the interpretation of fracture orientations and the thicknesses over which they predominate can be trusted for a more quantitative analysis.

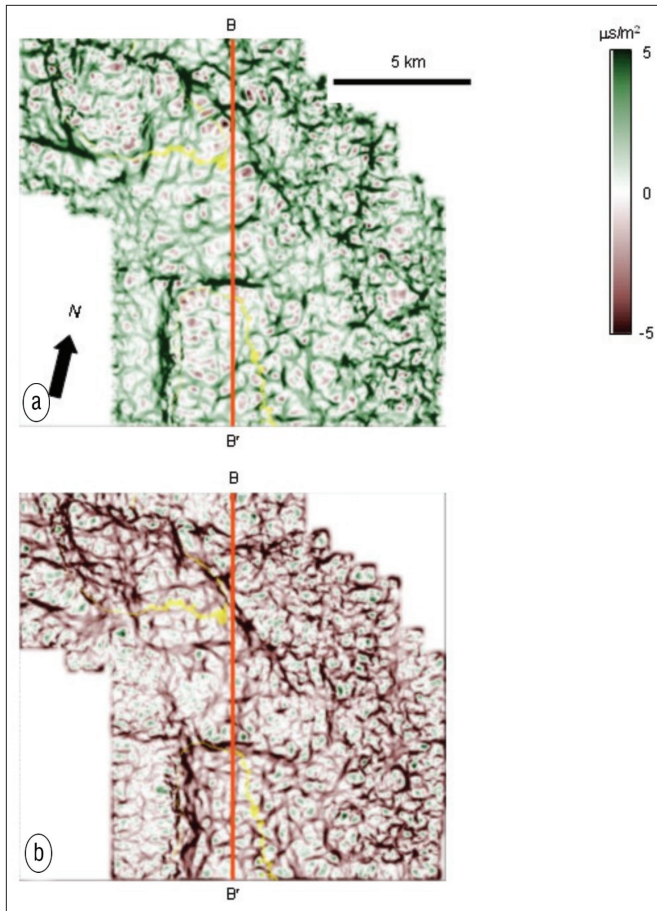


Figure 13. Time slice at 1.0 s through (a) most-negative and (b) most-positive curvature volumes. The yellow picks correspond to intersections of the time slice with the Thirty-one Formation shown in Figure 10a. Folds and flexures can be interpreted on these time slices prior to picking any horizons (after Marfurt, 2006).

Conclusions. Curvature attributes provide images of structure and stratigraphy that complement those seen by the well-accepted coherence algorithms. Being second-order derivative measures of surfaces, they can be quite sensitive to noise. Picks made on zero-crossings (on the quadrature of the data if appropriate) are in general less noisy than those made on peaks and troughs. Additional noise can be suppressed by iteratively running spatial filtering on horizon surfaces. Mean filters seem to do a satisfactory job and help enhance long-wavelength curvature features that may be difficult to see on the picked horizon itself. Median filters sharpen discrete horizon discontinuities such as faults.

For the data sets under study, strike curvature, shape index, most-positive, and most-negative curvature offered better interpretation of subtle fault detail than other attributes. Volume curvature attributes provide valuable information on fracture orientation and density in zones where seismic horizons are not trackable. The orientations of the fault/fracture lineations interpreted on curvature displays can be combined in the form of rose diagrams, which in turn can be compared with similar diagrams obtained from FMI data to gain confidence in calibration.

Suggested reading. “3D volumetric multispectral estimates of reflector curvature and rotation” by Al-Dossary and Marfurt (GEOPHYSICS, 2006). “3D seismic coherency for faults and stratigraphic features” by Bahorich and Farmer (TLE, 1995). “Improving curvature analyses of deformed horizons using scale-dependent filtering techniques” by Bergbauer et al. (AAPG Bulletin, 2003). “Volume-based curvature analysis illuminates fracture orientations” by Blumentritt (AAPG 2005 Annual Convention). *Seismic Attributes for Prospect Identification and Reservoir Characterization* by Chopra and Marfurt (SEG, in press). “Facies and curvature controlled 3D fracture models in a Cretaceous carbonate reservoir, Arabian Gulf” by Ericsson et al. (in *Faulting, Fault Sealing and Fluid Flow in Hydrocarbon Reservoirs*, Geological Society Special Publication 147, 1988).

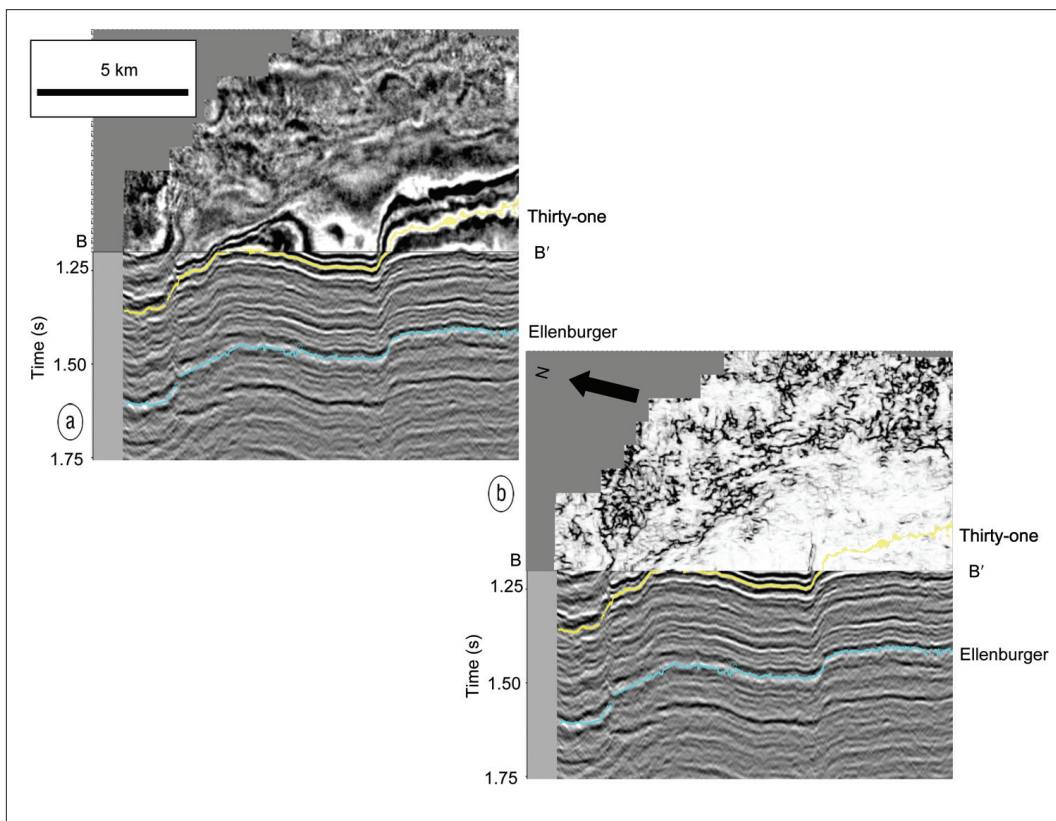


Figure 14. Cube-edge displays folded at 1.0 s along line AA' shown in Figure 11b, showing seismic on the vertical section and (a) seismic and (b) coherence on the time slice. The zone of intersection is relatively featureless on the coherence slice (after Marfurt, 2006).

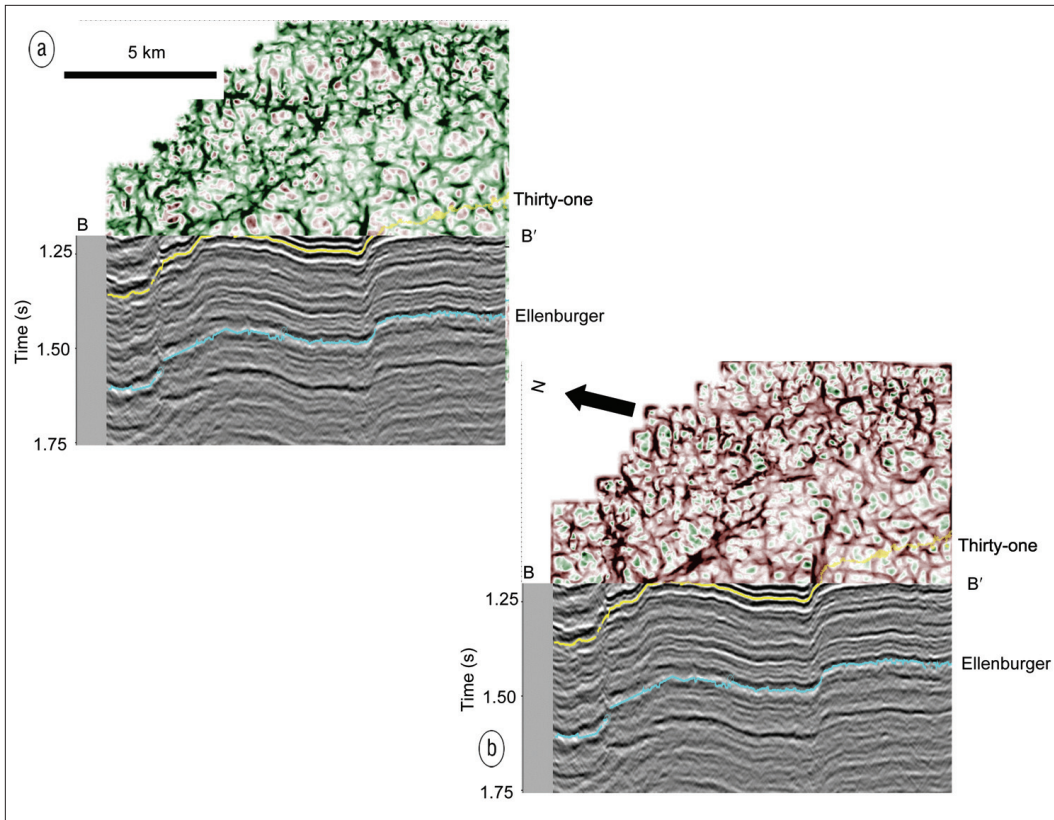


Figure 15. Cube-edge displays folded at 1.0 s along line AA' shown in Figure 11b, showing seismic on the vertical section and (a) most-negative and (b) most-positive curvature on the time slice. We can easily track folds and flexures seen on the seismic into the survey along the curvature slices (after Marfurt, 2006).

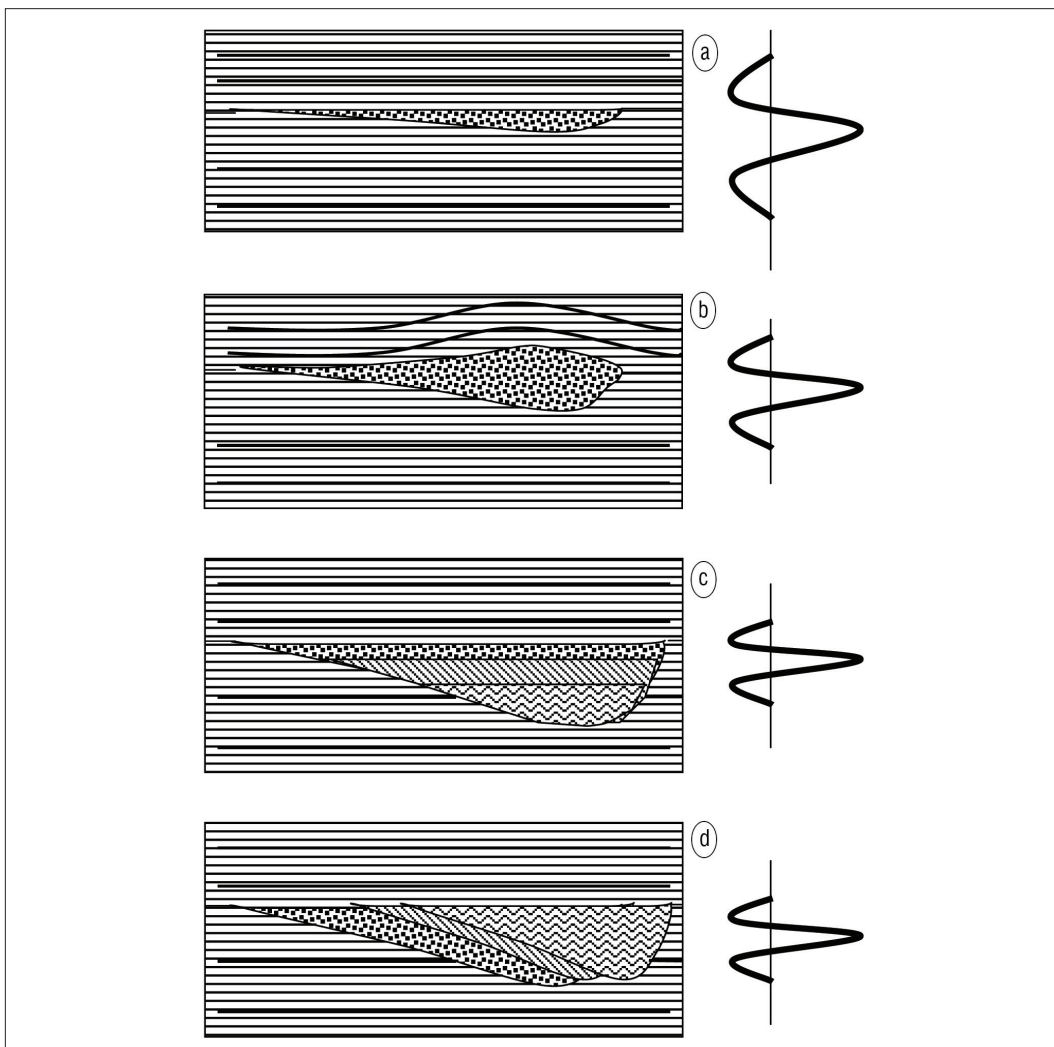


Figure 16. Attribute response to channel features preserved in the geologic record: (a) Below thin bed tuning. Homogeneous fill. No differential compaction. Change in amplitude only. (b) Below thin bed tuning. Homogeneous fill. Differential compaction. Change in curvature. Change in amplitude. No change in waveform. (c) Above thin bed tuning. Heterogeneous horizontal fill. No differential compaction. No change in curvature. Change in amplitude. Change in waveform. (d) Above thin bed tuning. Heterogeneous aggradational fill. Change in curvature, amplitude, and waveform.

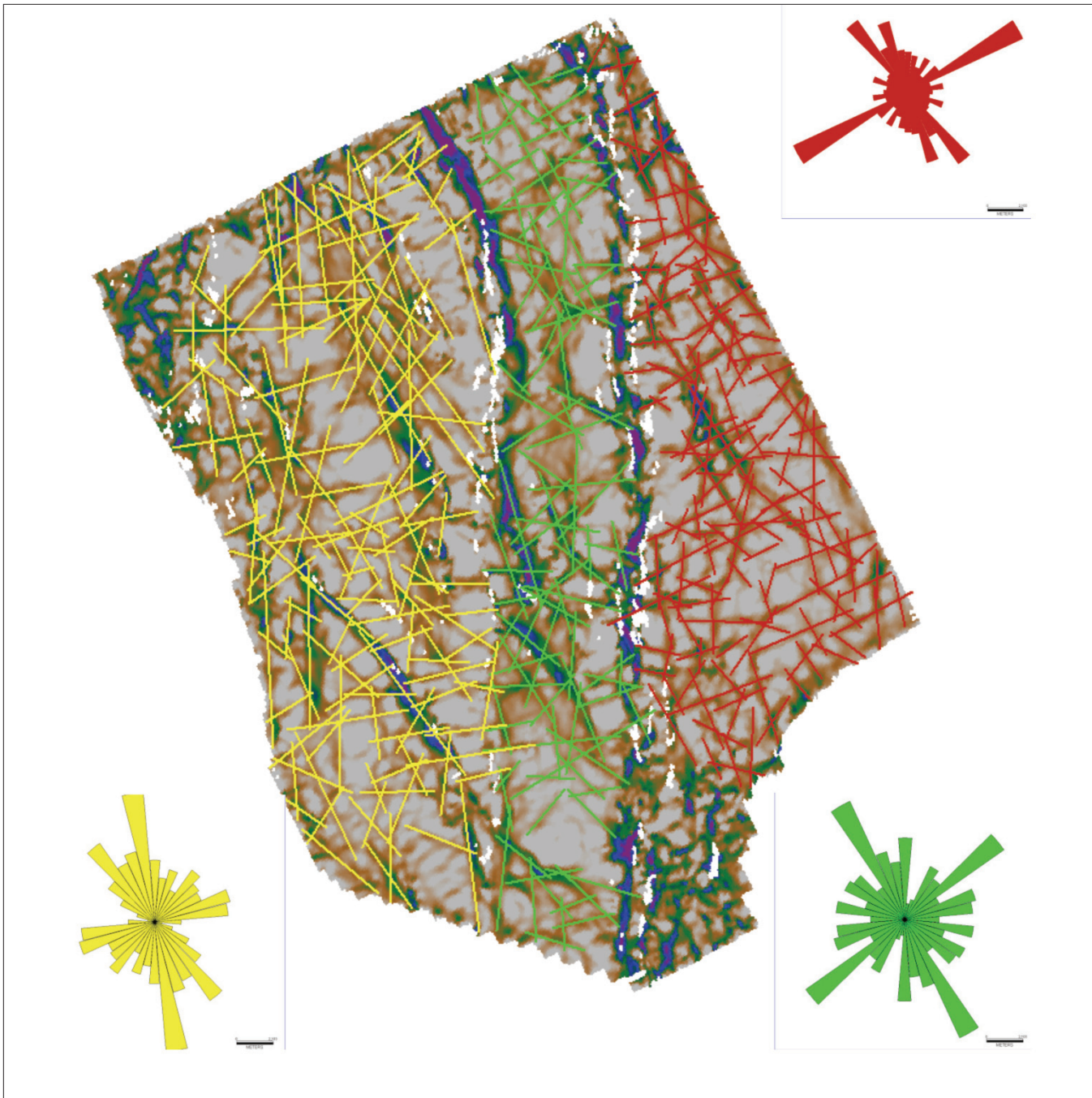


Figure 17. Interpretation of lineations corresponding to subtle faults carried out on the most-negative curvature horizon slice 120 ms below the horizon shown in Figure 4. The lineation interpretation is carried out on three separate compartments as distinguished by the two main faults running north-south and color. Rose diagrams prepared for the three sets of lineations are shown in their respective colors and can be compared with similar diagrams available from FMI logs (data courtesy of Arcis Corporation).

“Validating seismic attributes: Beyond statistics” by Hart (*TLE*, 2002). “Curvature attribute and seismic interpretation: Case study from Fort Worth Basin, Texas, U.S.” by Hakami et al. (SEG 2004 *Expanded Abstracts*). “3D seismic volume curvature attributes aid structural and stratigraphic interpretation” by Helmore et al. (2004 PETEX Conference). “Detection of zones of abnormal strains in structures using Gaussian curvature analysis” by Lisle (*AAPG Bulletin*, 1994). “Edge detection and stratigraphic analysis using 3D seismic data” by Luo et al. (SEG 1996 *Expanded Abstracts*). “Seismic Attribute Mapping of Structure and Stratigraphy” by Marfurt (SEG/EAGE DISC course, 2006). “Attribute extraction: An important application in any detailed 3D interpretation study” by Rijks and Jauffred (*TLE*, 1991).

“Curvature attributes and their application to 3D interpreted horizons” by Roberts (*First Break*, 2001). “The Austin Chalk: Simulation of horizontal wells in a heterogeneous formation” by Schnerk and Madeen (SPE 20716, 2000). “Curvature attributes and seismic interpretation: Case studies from Argentina basins” by Sigismondi and Soldo (*TLE*, 2003). **TLE**

Acknowledgments: We thank Chuck Blumentritt of Geotexture Technologies for processing the volume curvature attributes and preparing the image shown in Figure 17. We thank Arcis Corporation for permission to show the data examples and publish this work.

Corresponding author: schopra@arcis.com